

Article

Biowaste-Derived Heteroatom-Doped Porous Carbon as a Sustainable Electrocatalyst for Hydrogen Evolution Reaction

Raji Atchudan ^{1,*},, Suguna Perumal ^{2,†},, Thomas Nesakumar Jebakumar Immanuel Edison ^{3,†},
Ashok K. Sundramoorthy ^{4,†},, Namachivayam Karthik ⁵, Sambasivam Sangaraju ⁶,, Seung Tae Choi ⁵,
and Yong Rok Lee ^{1,*}

¹ School of Chemical Engineering, Yeungnam University, Gyeongsan 38541, Republic of Korea

² Department of Chemistry, Sejong University, Seoul 143747, Republic of Korea

³ Department of Chemistry, Sethu Institute of Technology, Kariapatti, Virudhunagar District 626115, Tamil Nadu, India

⁴ Department of Prosthodontics, Saveetha Dental College and Hospitals, Saveetha Institute of Medical and Technical Sciences, Poonamallee High Road, Velappanchavadi, Chennai 600077, Tamil Nadu, India

⁵ Functional Materials and Applied Mechanics Lab, School of Mechanical Engineering, Chung-Ang University, Seoul 06974, Republic of Korea

⁶ National Water and Energy Center, United Arab Emirates University, Al Ain 15551, United Arab Emirates

* Correspondence: atchudanr@yu.ac.kr (R.A.); yrlee@yu.ac.kr (Y.R.L.)

† These authors contributed equally to this work.

Abstract: Heteroatom-doped porous carbon material (H-PCM) was synthesized using *Anacardium occidentale* (cashew) nut's skin by a simple pyrolysis route. The resulting H-PCM was thoroughly characterized by various analytical techniques such as field emission scanning electron microscopy (FE-SEM) with energy-dispersive X-ray (EDX) spectroscopy, high-resolution transmittance electron microscopy (HRTEM), X-ray diffraction (XRD), Raman spectroscopy, nitrogen adsorption-desorption isotherms, X-ray photoelectron spectroscopy (XPS), and attenuated total reflectance Fourier transform infrared (ATR-FTIR) spectroscopy. The obtained results strongly demonstrated that the synthesized H-PCM exhibited a porous nature, continuous sponge-like and sheet-like smooth morphology, and a moderate degree of graphitization/crystallinity with oxygen-, nitrogen-, and sulfur-containing functionalities in the carbon matrix. After the structural confirmation, as-prepared H-PCM has used a sustainable electrocatalyst for hydrogen evolution reaction (HER) because the metal-free carbonaceous catalysts are one of the most promising candidates. The H-PCM showed excellent HER activities with a lowest Tafel slope of 75 mV dec⁻¹ and durable stability in 0.5 M H₂SO₄ aqueous solution. Moreover, this work provides a versatile and effective strategy for designing excellent metal-free electrocatalysts from the cheapest biowaste/biomass for large-scale production of hydrogen gas through electrochemical water splitting.

Keywords: cashew nut; pyrolysis; porous carbon; electrocatalyst; hydrogen evolution reaction; clear/green energy



Citation: Atchudan, R.; Perumal, S.; Jebakumar Immanuel Edison, T.N.; Sundramoorthy, A.K.; Karthik, N.; Sangaraju, S.; Choi, S.T.; Lee, Y.R. Biowaste-Derived

Heteroatom-Doped Porous Carbon as a Sustainable Electrocatalyst for Hydrogen Evolution Reaction.

Catalysts **2023**, *13*, 542. <https://doi.org/10.3390/catal13030542>

Academic Editors: Sekar Karthikeyan and Boopathy Ramasamy

Received: 30 December 2022

Revised: 23 February 2023

Accepted: 2 March 2023

Published: 8 March 2023



Copyright: © 2023 by the authors. Licensee MDPI, Basel, Switzerland. This article is an open access article distributed under the terms and conditions of the Creative Commons Attribution (CC BY) license (<https://creativecommons.org/licenses/by/4.0/>).

1. Introduction

Recently, nanomaterials with different architectures and supports have played a key role in industrial catalysis. Electrocatalysts are a variety of catalysts, which participate in a selective electrochemical reaction to increase the reaction rate of redox processes at the electrode/electrolyte interface. The electro-catalytic processes can occur at the electrode surface or electrode itself [1,2]. In recent days, various electro-catalytic reactions including oxygen reduction reaction (ORR), oxygen evolution reaction (OER), hydrogen evolution reaction (HER), and carbon dioxide reduction reactions are significantly important due to their involvement in green energy and environment-based applications [3,4]. Particularly, electro-catalytic HER is mainly focused on the bulk production of hydrogen gas

through water splitting. Platinum and platinum-based composites are served as benchmark electrocatalysts for HER in all pH ranges. The scarceness and expense of platinum-based electrocatalysts hinder their applicability [5–9]. Hence, the replacement of noble platinum is necessary with cost-effective materials. Recent studies proved that nitrogen-doped carbon materials act as good electrocatalysts for HER and ORR reactions [10–12].

Carbon is capable of forming more than one crystalline form due to its valency, which is called allotropes of carbon. Graphite, diamond, and amorphous carbon are the most common allotropes of carbon. Depending on the arrangement of atoms the properties of allotropes can vary [13]. The crystal structure of diamond is an infinite three-dimensional array of carbon atoms, which makes less chemical reactivity, extreme hardness, and insulating properties of diamond, whereas the crystal structure of graphite amounts to a parallel stacking of layers of carbon atoms leads to the fascinating properties such as good electrical conductivity, softness, and lubricity of graphite [14,15]. The electrical conductivity, defects, and porosity of carbon materials can be easily tuned by the doping of electron-rich heteroatoms including nitrogen, oxygen, sulfur, and boron. Hence, the heteroatom-doped carbon materials received great attention from researchers owing to their excellent electrical conductivity, optical properties, and capacitive behavior which helps the applicability of heteroatom-doped carbon materials in catalysis, electrocatalysis, energy storage, and fluorescent sensors [16–18]. Particularly, nitrogen-doped carbon nanoparticles have competed with other heteroatom-doped carbon nanomaterials due to their applicability in energy-related applications including water-splitting reactions HER, OER, and ORR.

The nitrogen-doped carbon materials can be synthesized by pyrolyzation of green carbon sources such as glucose, citric acid, dried plant parts, and biowastes under the nitrogen atmosphere. This method provides various benefits including cost-effectiveness and a simple experimental setup [19,20]. Sun et al. reported the synthesis of nitrogen-doped porous carbon using orange peel by carbonization using a tube furnace under the nitrogen atmosphere [21]. Sekhon and Park conducted an excellent review on biomass-derived nitrogen-doped porous carbon nanosheets for energy technologies [22]. Moreover, Matsagar et al. reviewed the recent progress of biomass-derived nitrogen-doped porous carbon and its applications [23]. Chen et al. described that nitrogen/sulfur-doped porous graphene displayed enhanced electro-catalytic activity towards HER that was comparable to that of commercial electrocatalysts such as Pt-free MoS₂ catalysts [24,25]. Many authors utilized natural green biowastes/biomass for the synthesis of carbon materials [26–28].

Here, porous carbon materials were synthesized using cost-effectiveness and a greener route. The present study involved the synthesis of heteroatom-doped porous carbon material (H-PCM) using *Anacardium occidentale* (cashew) nut's skin (CNS) by a simple pyrolysis route under the nitrogen atmosphere. The CNS contains several phytoconstituents and is easily accessible at a low cost. The corresponding phytoconstituents can act as the source of carbon, nitrogen, oxygen, and sulfur for the formation of a carbon matrix during the pyrolysis process. The synthesized H-PCM was characterized by various surface- and structure-confirming analytical tools. Further, the synthesized H-PCM are coated on carbon cloth and used as electrocatalysts for HER in acid media. The HER reaction is monitored by linear sweep voltammetry, electrochemical impedance spectroscopy (EIS), and Tafel methods. Moreover, this investigation throws light on the mere future for more possibilities to transform solid waste into environmentally friendly energy conversion.

2. Results and Discussion

The morphologies investigation of the synthesized porous carbon material was thoroughly studied using FE-SEM with energy-dispersive X-ray (EDX) spectroscopy, selected area electron diffraction (SAED), and TEM measurements were performed. The FE-SEM images of H-PCM (Figure 1a–e) displayed the porous structure with interconnected channels that might be favored for the transport of electrolytes. In addition, the presented pores facilitate the easy release of bubbles that are produced during the HER. Figure 1f–k displays the FE-SEM images and their corresponding elemental mapping of H-PCM. Carbon, oxy-

gen, nitrogen, and sulfur have been detected in the H-PCM from the elemental mapping measurements. The presented heteroatoms were distributed uniformly throughout the carbon matrix. Furthermore, as shown in Figure 11, the elemental composition of the synthesized H-PCM was further confirmed from the EDX spectrum. The spectrum demonstrated that the H-PCM exhibits carbon, oxygen, nitrogen, and sulfur elements. Apart from these essential elements, silicon, and platinum are presented in the spectrum, silicon is from silicon wafers that are used as substrate, and platinum that used for coating.

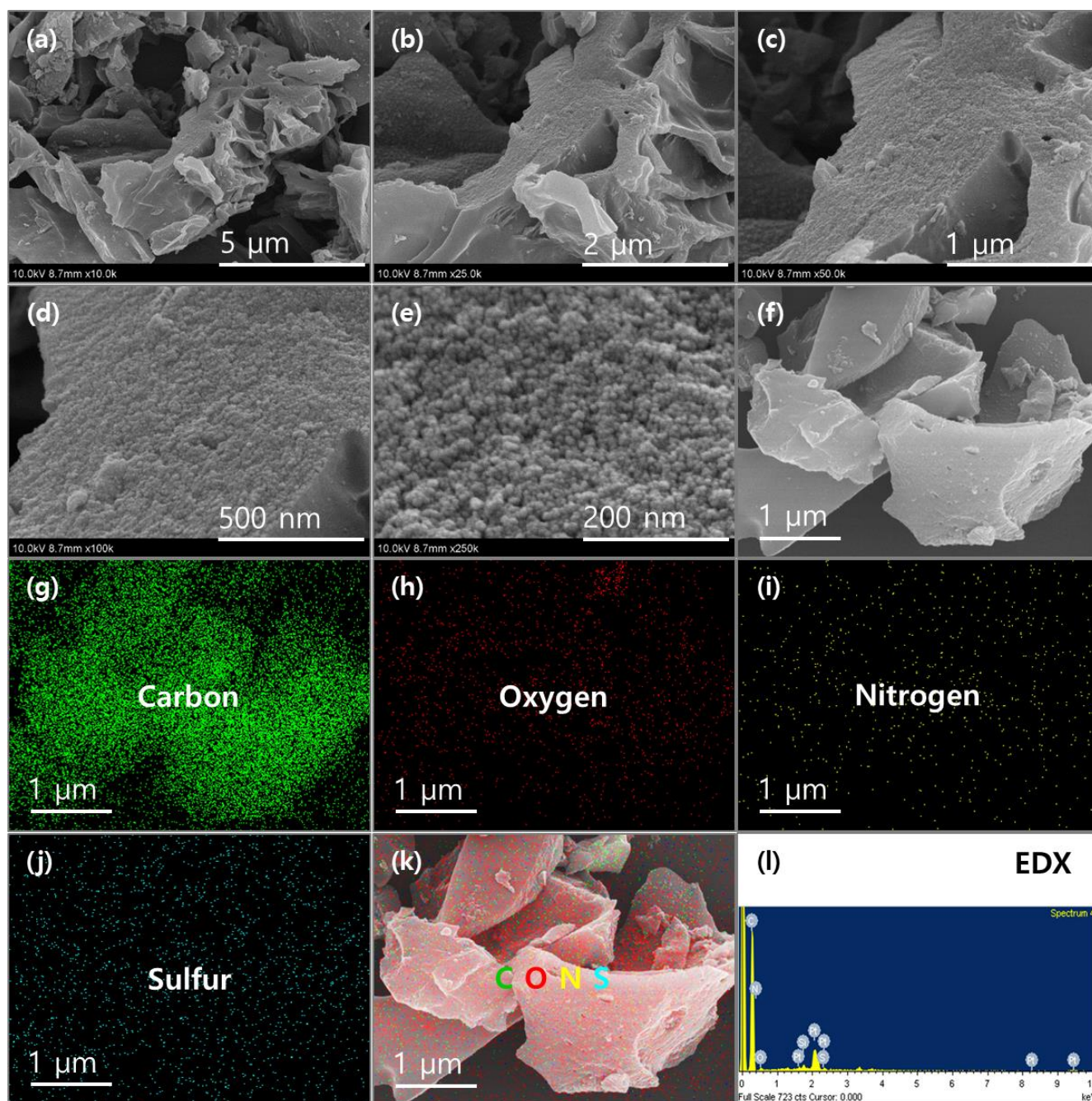


Figure 1. (a–e) FE-SEM images at different magnifications of synthesized H-PCM; (f) FE-SEM electron image of synthesized H-PCM and the corresponding EDX mapping of (g) carbon, (h) oxygen, (i) nitrogen, (j) sulfur, and (k) overlapping of all the presented elements; (l) EDX spectrum results of presented elements in the synthesized H-PCM.

Further, the overall morphology and porous structure of the synthesized H-PCM were revealed by TEM/HRTEM analysis. Figure 2a–c shows the TEM images of synthesized H-PCM with different magnifications. These images demonstrated that the H-PCM exhibits a mixture of continuous sponge-like and sheet-like architecture with many disordering interconnected porous textures [29,30]. The obviously observed pores are distributed in the range of approximately several nanometers, and this is in favor of the rapid transport of electrolytes which might be facilitated the electrochemical reaction toward HER. HRTEM image (Figure 2d) shows indistinct lattice fringes with a typical turbostratic structure which revealed the partial graphitization of synthesized H-PCM. The existence of abundant heteroatom-containing functional groups mitigates the degree of graphitization. It was expected that this outstanding nature of H-PCM will enhance the electric conductivity and will be a potential candidate for electrochemical reactions [31]. Furthermore, the analysis of SAED confirms the degree of crystallinity/graphitic nature of materials. The inset of Figure 2d depicts the dim narrow rings suggesting partial graphitization/crystallinity of H-PCM.

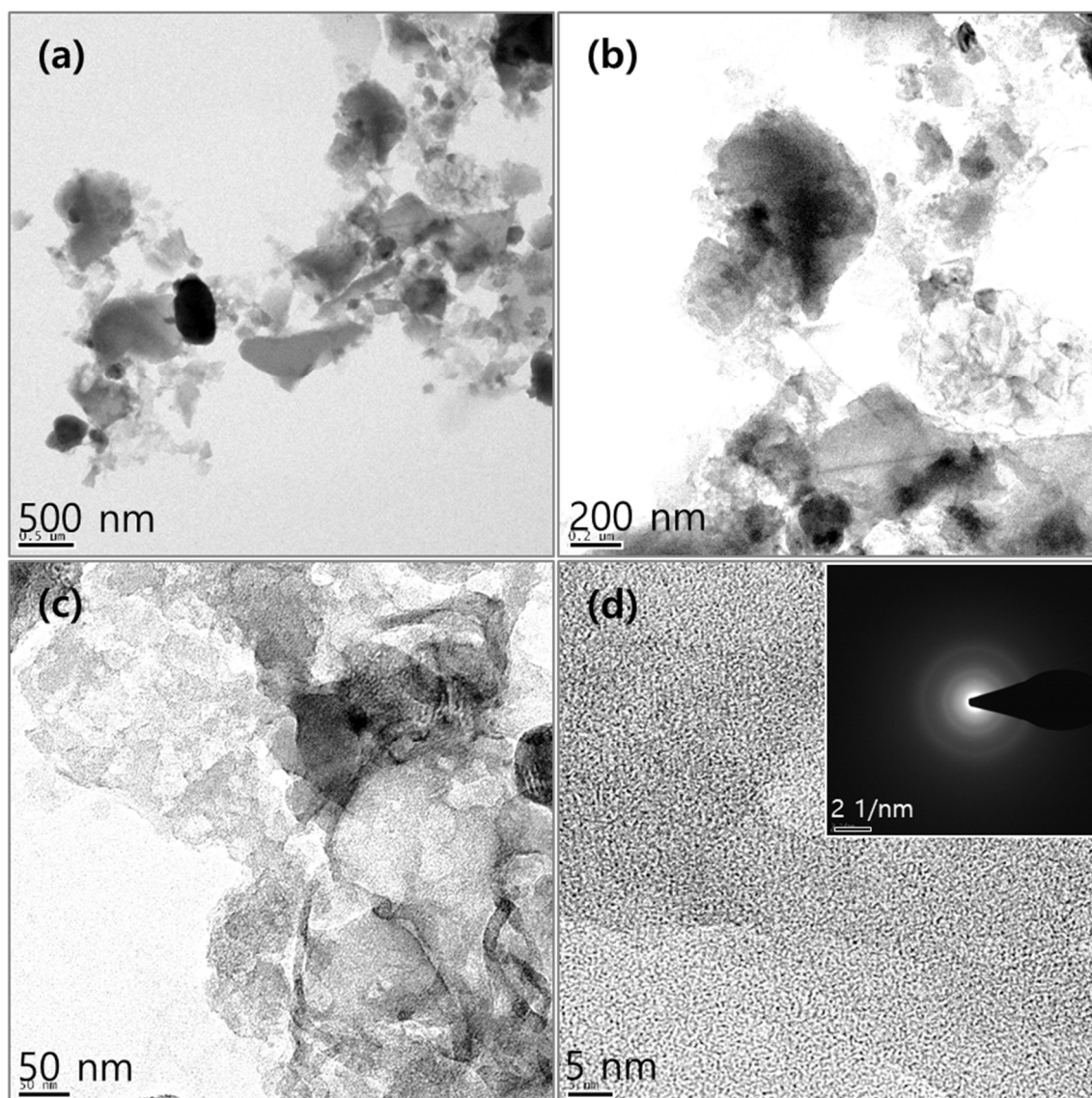


Figure 2. (a–d) TEM/HRTEM images at different magnifications of synthesized H-PCM (inset (d): SAED pattern of H-PCM).

Figure S1 demonstrates the XRD pattern of H-PCM synthesized using CNS waste. The XRD peaks positioned at $2\theta = 26$ and 44° correspond to the reflections of the (002) and (100) planes for the characteristic graphitic carbon, respectively [32–34]. The absence of sharpness in the two diffraction peaks ($2\theta = 26$ and 44°) indicates that the H-PCM partial graphitic state/disordered carbon structure, and also might have smaller carbon sheets. This result coincides well with the TEM results. Apart from these two distinguished peaks ($2\theta = 26$ and 44°) that are responsible for graphitic carbon, many other minor peaks were observed. The minor peaks might be from the phytoconstituents and minerals from the biomass/biowaste materials. The quality of the carbon materials in respect of the graphitization of synthesized H-PCM was further evaluated by Raman spectroscopy. Raman spectra of H-PCM (Figure 3a) exhibit two major peaks positioned at 1345 and 1595 cm^{-1} are attributed to the D- and G-bands, respectively [35,36]. The D-band is correlated to the breathing mode of defective/disordered (sp^3) carbon, whereas the G-band corresponds to the vibration mode of the graphitic/crystalline (sp^2) carbon [37]. The slightly low intensity of the graphitic band (G-band) compared to the D-band can be due to the existence of functional groups. The relation between the intensity of the D-band and G-band (I_D/I_G) determined the graphitization/crystallinity and arrangement of the graphene planes in the synthesized H-PCM [38]. The I_D/I_G value of H-PCM was calculated as 1.03, which implies the partial graphitization/crystallinity and structural defects that might be due to the porosity as well as because of the doping of heteroatoms/heteroatoms-containing functionalities. Apart from these two major peaks, the low intense and broad Raman vibration is located around 2800 cm^{-1} and is denoted as a 2D-band which is a fingerprint of graphene order (number of graphene sheets) in the H-PCM [39,40]. In the case of unclear separation between the D-band and G-band, the determination of graphitization/crystallinity is complicated. Hence, the Raman spectrum of H-PCM was deconvoluted, and the graphitization/crystallinity was determined by the area of the D-band and G-band (A_D and A_G). The ratio of A_D/A_G was calculated as 0.95 (Figure 3b), which indicates the acceptable graphitic order of H-PCM. Overall results strongly revealed that the synthesized H-PCM exhibit graphitic order with partial structural defects.

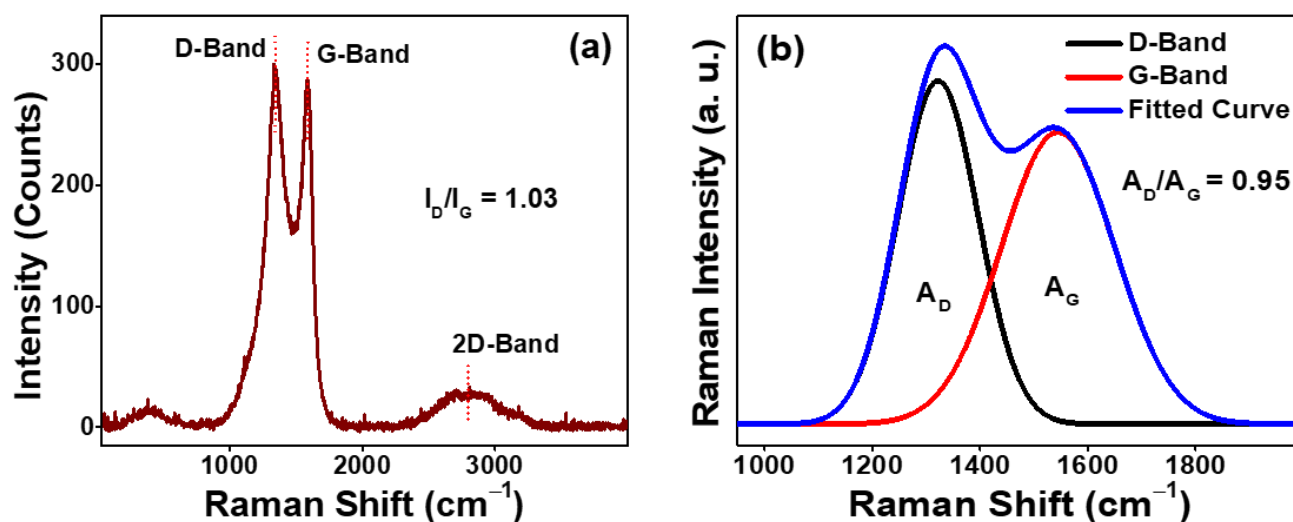


Figure 3. (a) Raman spectrum and (b) Raman spectrum with deconvolution of D-band/G-band of synthesized H-PCM.

ATR-FTIR spectroscopy is used to study the chemical composition and surface functional groups on the synthesized H-PCM. Figure S2 shows the ATR-FTIR spectrum of as-synthesized H-PCM. The characteristic absorption bands at 3375 cm^{-1} belong to the stretching vibration of O–H groups on the H-PCM surface [41]. The N–H stretching vibration of H-PCM appeared around 3100 cm^{-1} [42]. The absorption peaks of H-PCM around 2835 and 2700 cm^{-1} are overlapped and displayed as a broader band which belongs to

the C–H and S–H stretching vibrations, respectively. The ATR-FTIR spectrum of H-PCM exhibits absorption bands at 2362 and 2332 cm^{-1} , which can be accredited to the stretching vibration of atmospheric $-\text{CO}_2$ and $-\text{C}\equiv\text{N}$ functional groups, respectively. The absorption bands at 2106 and 1650–1850 cm^{-1} correspond to the stretching vibration of $-\text{C}=\text{N}$ and $\text{C}=\text{O}$ functional species. The absorption peak at 1580 cm^{-1} is assigned to the stretching vibration of sp^2 carbon bonding ($\text{C}=\text{C}$) in the porous carbon matrix of the H-PCM [43]. The stretching vibration bands of C–N/C–S are located in a range of 1330–1420 cm^{-1} . The absorption bands in the area between 1120 and 1000 cm^{-1} might be ascribed to the stretching vibrations of C–OH (alkoxy) and C–O–C (epoxy) functional groups, respectively [44]. The out plane aromatic ring stretching vibration of the $-\text{CH}_2$ band emerged at 826 cm^{-1} in the ATR-FTIR spectrum of the H-PCM [45]. The absorption peaks located at 710 and 616 cm^{-1} correspond to the stretching vibrations of the C–S groups [46]. The absorbance peak at 470 cm^{-1} corresponds to the S–O stretching vibrations in the porous carbon framework. The ATR-FTIR spectral results show that elements such as carbon, oxygen, nitrogen, and sulfur are exhibited in the synthesized H-PCM which suggests the heteroatoms doping into the H-PCM.

The XPS is used to further investigate the chemical composition and elemental state of surface groups on H-PCM. As shown in Figure S3, the synthesized H-PCM mainly contains carbon, oxygen, nitrogen, and sulfur with atomic percentages of 67, 28, 3, and 2, respectively. The high-resolution XPS spectrum of C 1s (Figure 4a) exhibits five main peaks at 284.1 eV, corresponds to the carbon-bonded with hydrogen (C–H), 284.8 eV credited to the signal of disorder sp^3 -bonded carbon and graphitic sp^2 -bonded carbon, 285.8 eV confirms the C–O (epoxy and alkoxy), C–N, and C–S functionalities, 286.6 eV suggests the presence of carbonyl groups ($\text{C}=\text{O}$), and 287.5 eV, attributed to carboxyl species ($\text{H}-\text{OC}=\text{O}$) [6,47–49]. The existence of graphitic sp^2 ($\text{C}=\text{C}$) bonds and epoxy/alkoxy (C–O–C/C–O–H) bonds might enhance expectations of the electric conductivity of electrocatalysts (H-PCM). The high-resolution O 1s spectrum can be deconvoluted (Figure 4b) into three distinct binding energy peaks at 531.3, 532.5, and 533.6 eV that are accredited to the $\text{C}=\text{O}$, C–O/S–O, and $\text{O}=\text{C}-\text{O}$ functional species, respectively [39,50]. The high-resolution N 1s spectrum can be deconvoluted into three peaks positioned at binding energies of 398.9, 400.8, and 404.1 eV, which were credited to the C–N–C (pyridinic), C–N–H (pyrrolic), and C_3-N (quaternary N atoms) functional moieties, respectively [51,52]. The presence of C–N proves that nitrogen was incorporated successfully into the porous carbon matrix of H-PCM. The high-resolution S 2p spectrum can be divided into four binding energy peaks by deconvolution. The peaks appeared at 164.1 and 165.3 eV, corresponding to S 2p_{3/2} and S 2p_{1/2}, respectively, suggesting the possibility of aromatic C–S–C and C=S functionalities [53,54]. The C–S–C group profoundly demonstrates that the H-PCM is successfully doped with sulfur [55]. Other binding energy peaks positioned at 168.8 and 169.9 eV suggests the existence of oxidized sulfur (OS) in the form of $\text{OS}_{3/2}$ and $\text{OS}_{3/2}$, respectively; basically present C–SO–C (sulfoxide) and C–SO₂–C (sulfone) in the H-PCM [56,57]. The aromatic C–S–C and C=S functionalities could modify the atmosphere of the porous carbon surface/edges and improve the total polarization of the medium [57]. The incidence of sulfur species can also enhance electrochemical reactions by increasing the conductivity of the carbon matrix. These findings of heteroatom functionalities are consistent with FT-IR results. Thus it was believed that the HER performance would be enhanced by the presence of heteroatoms [58].

The numerous number of micropores and mesopores is one of the key factors in determining the electrochemical activity by easily allowing electrolytes and strong holding of heteroatoms during the electrochemical reaction. Nitrogen sorption (adsorption–desorption) measurements were performed on the synthesized H-PCM under standard temperature and pressure. As shown in Figure S4, the synthesized H-PCM exhibited a combination of type I and type IV isotherm characteristics in nature with a type H4 hysteresis loop appearance that indicates acceptable pores with a layered structure in the carbon matrix of H-PCM. The characteristic type I isotherms were displayed in the lower relative pressure ($P/P_0 < 0.1$) with high nitrogen adsorption quantity in a vertical design, suggesting that

H-PCM possessed a higher number of micropores [59]. The nitrogen sorptions relative pressure (P/P_0) within the range from 0.2 to 0.9 represents the type IV isotherms with an H4 hysteresis loop, indicating that the H-PCM had mesoporous adsorption characteristics nature [60]. The isotherms that appeared with higher relative pressure ($P/P_0 > 0.9$) represent the macropores that originated from slit holes in the carbon structure and wide spacing within the layered structure of H-PCM. The combination of isotherms type I and IV indicated that the synthesized H-PCM contains adequate porous structures including micropores, mesopores, and macropores. Micropores and mesopores are responsible for the higher specific surface area, whereas macropores also help to transport chemical components. The presented porosity of synthesized H-PCM has been verified by the FESEM and TEM/HRTEM observations. The obtained Brunauer–Emmett–Teller (BET) surface area of synthesized H-PCM was $565 \text{ m}^2 \text{ g}^{-1}$. These porous structures with high surface presented H-PCM is more beneficial for the electrons and ions which resulting enhanced electro-catalytic activity towards HER [61].

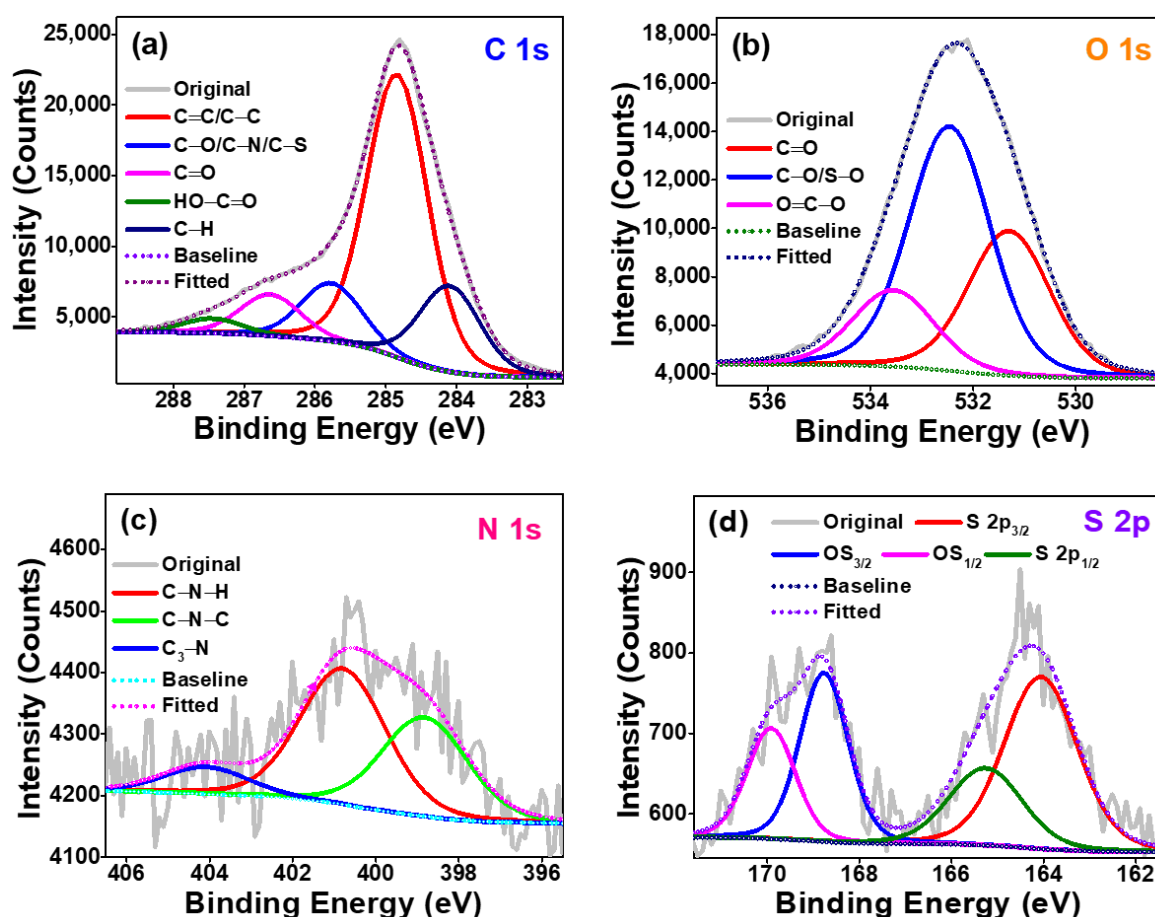


Figure 4. XPS high-resolution spectra with deconvolution peaks of (a) C 1s, (b) O 1s, (c) N 1s, and (d) S 2p regions of synthesized H-PCM.

The HER performance was examined using synthesized H-PCM as a catalyst in $0.5 \text{ M H}_2\text{SO}_4$ aqueous solution under atmospheric conditions. The linear sweep voltammetry studies of H-PCM-adorned carbon cloth (H-PCM/CC) are performed at the scan rate of 10 mV s^{-1} and the corresponding polarization curves are presented in Figure 5a and Figure S5. As shown in Figure 5a and Figure S5, the cathodic current density (CCD) of the unadorned carbon cloth did not alter much upon increasing the negative potential, suggesting the lower catalytic activity of bare carbon cloth. Whereas, the CCD of the synthesized H-PCM/CC increased quickly by increasing the negative potential, indicating that the synthesized H-PCM possessed higher catalytic activity toward HER [59]. The initial

potential of the bare platinum plate (standard catalyst) was nearing zero, and the delivered lowest overpotential ($70 \text{ mV}_{\text{RHE}}$) at a CCD of 10 mA cm^{-2} , while unadorned carbon cloth has negligible HER activity (overpotential: $918 \text{ mV}_{\text{RHE}}$). The synthesized H-PCM catalyst delivered an overpotential of $133 \text{ mV}_{\text{RHE}}$ at a CCD of 10 mA cm^{-2} that is comparable to that of the bare platinum catalyst. The synthesized H-PCM (H-PCM/CC) catalyst exhibits high catalytic activity toward HER compared to bare carbon cloth. The doping of heteroatoms including nitrogen and sulfur possibly enhanced the electro-catalytic activities of the synthesized H-PCM. The Tafel slope of the catalyst is one of the significant parameters for determining the HER performance. The Tafel slope of H-PCM/CC is 75 mV dec^{-1} in the HER process follows the Volmer–Heyrovsky mechanism (Figure 5b) [62]. The lowest Tafel slope of H-PCM-adorned carbon cloth implies fast reaction kinetics of synthesized H-PCM catalyst towards HER [63]. Moreover, the lower Tafel slope of H-PCM suggests their excellent catalytic performances. Even though the Tafel slope is greater than that of the bare platinum catalyst, that is comparable to or lower than that of earlier reports (Table 1).

EIS is one of the significant tools for studying electro-catalytic materials in terms of examining the electrode and electrolyte interface reaction including charge transfer resistance and coating effect. The EIS Nyquist plot of the synthesized H-PCM electrode (H-PCM/CC) was measured at open circuit potential in $0.5 \text{ M H}_2\text{SO}_4$ aqueous solution, and obtained results were fitted (Figure 5c). As shown in the EIS Nyquist plot, the charge transfer resistance of H-PCM/CC is around $1.9 \Omega \text{ cm}^{-2}$. The lowest charge transfer resistance for the H-PCM/CC working electrode demonstrated that the synthesized H-PCM exhibits faster reaction kinetics which can result in excellent HER. The highest HER performance might be due to the comparable degree of graphitization, high surface area with acceptable porosity, and heteroatom-containing rich functionalities. In addition, the EIS Nyquist plot is nearly perpendicular to the y-axis, suggesting the good conductance of the prepared electrocatalyst (H-PCM). The recorded EIS Nyquist plot is perfectly fitted with the proposed equivalent circuit as shown in the inset of Figure 5c [6]. Furthermore, the EIS Nyquist plots are recorded at different overpotentials ($0.57, 0.47, 0.37, 0.27, 0.17, 0.07, -0.03$, and $-0.13 \text{ V}_{\text{RHE}}$), which are shown in Figure 5d. The EIS Nyquist plots displayed that charge transfer resistance gradually decreased while increasing the overpotential, suggesting the kinetics of HER depends on the supplied potential. Notably, the higher HER performance occurred at the higher overpotential.

The stability of the synthesized electrocatalyst is one of the essential criteria for the applicability of real-time applications. Hence, the long-term durability measurement of synthesized H-PCM is performed by the chronoamperometry method at a controlled potential of $-0.15 \text{ V}_{\text{RHE}}$, as shown in Figure 6a. The durability test was conducted in $0.5 \text{ M H}_2\text{SO}_4$ aqueous solution for 24 h, and the retention rate of current density was maintained at nearly 100% compared to the initial current density, manifesting that the H-PCM was remarkably stable [64]. Nitrogen and sulfur-rich carbon materials showed remarkable catalytic activity toward HER with outstanding stability [65]. The linear sweep voltammetry polarization curve of the H-PCM/CC electrode was again recorded at the scan rate of 10 mV s^{-1} after the completion of the stability study. The obtained linear sweep voltammetry polarization curve was compared with the initial linear sweep voltammetry polarization curve of the H-PCM/CC electrode (Figure 6b). There is no significant difference in both linear sweep voltammetry polarization curves (before and after stability), authenticating that the synthesized H-PCM is greatly stable and could be a potential candidate as an electrocatalyst for HER in the acidic media. In addition, the EIS Nyquist plot of the synthesized H-PCM electrode measured at open circuit potential in $0.5 \text{ M H}_2\text{SO}_4$ aqueous solution after the prolonged stability and obtained results were compared to before the prolonging stability. Figure S6 shows the EIS Nyquist plots of synthesized H-PCM electrodes obtained before and after prolonged stability. The EIS Nyquist plots exhibit insignificant changes before and after, suggesting excellent stability in the acidic medium towards HER. Aforesaid, all the analytical results strongly imply that the synthesized H-PCM catalyst (metal-free electrocatalyst) had great application value toward HER in the acidic medium.

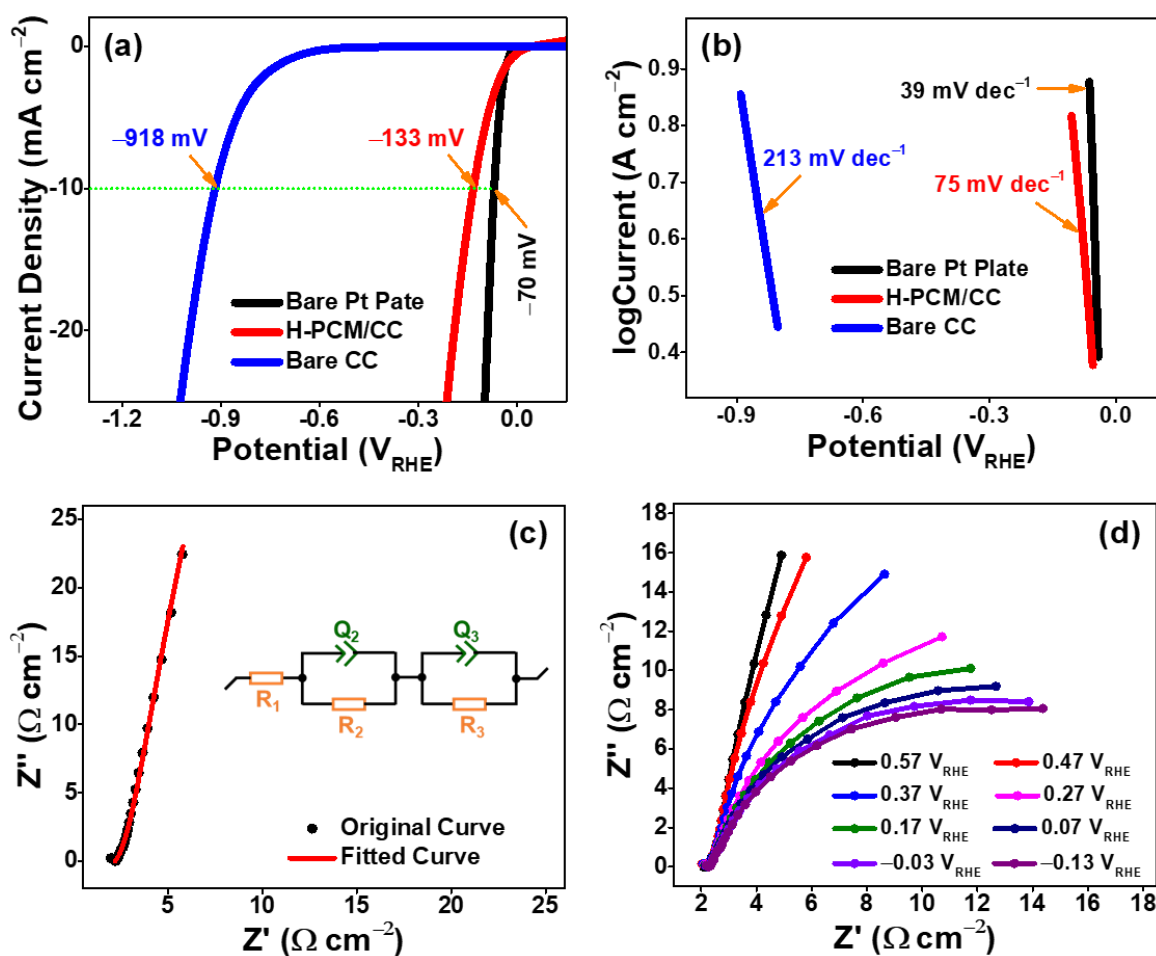


Figure 5. Electro-catalytic studies of synthesized H-PCM, bare platinum plate, and bare carbon cloth electrodes in 0.5 M H_2SO_4 aqueous solution towards HER under static atmosphere; (a) linear sweep voltammetry polarization curves at the scan rate of 10 mV s^{-1} , (b) Tafel plots, (c) EIS Nyquist plot and suitable fitting with the equivalent circuit of H-PCM electrode recorded at open circuit potential, and (d) EIS Nyquist plot of H-PCM electrode at different overpotentials.

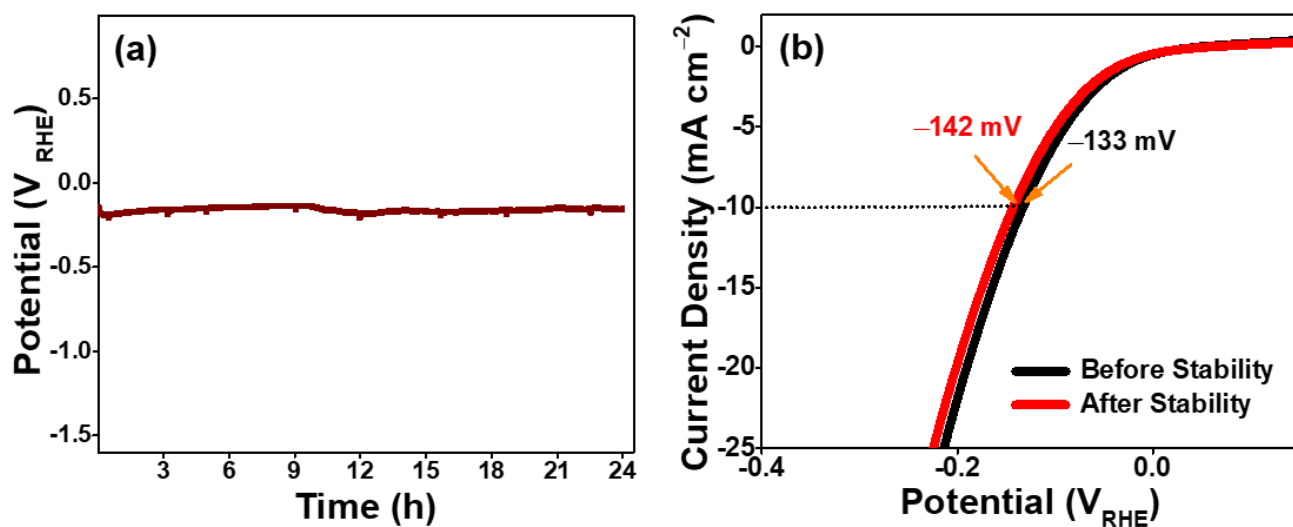


Figure 6. (a) Stability curve of synthesized H-PCM electrode was recorded in 0.5 M H_2SO_4 aqueous solution towards HER for 24 h and (b) linear sweep voltammetry polarization curves of synthesized H-PCM electrode obtained before and after prolonged stability.

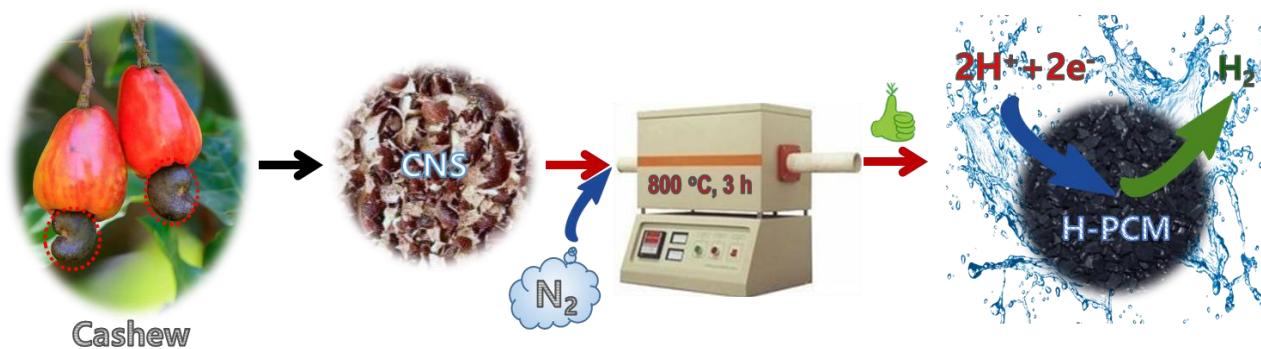
Table 1. The HER performances of H-PCM were compared with the reported ones.

Electrocatalysts	Preparation Method	Overpotential at 10 mA cm ⁻² (mV)	Tafel Slope (mV dec ⁻¹)	Reference
SrTiO ₃ @MoS ₂	Calcination	165	81.41	[66]
NA9	Carbonization	184	164	[67]
NPCF	Annealing	248	135	[64]
S-MoS ₂ /rGO/CNTs	Carbonization	159	85	[68]
Mo ₂ C/C	Pyrolysis	133	71	[69]
LS-PC	Pyrolysis	135	85	[45]
PS/MoS ₂	Pyrolysis	154	71	[70]
Porous Mo ₂ C/C	Sintering	556	123.9	[59]
Ni/P-doped carbon	Pyrolysis	297	134.9	[71]
BS-800	Calcination	413	98	[72]
H-PCM	Pyrolysis	133	75	This work

3. Materials and Methods

Synthesis of Heteroatom-Doped Porous Carbon Material

CNS waste was dried in sunlight, then it was made into a fine powder using a commercial mixer grinder. The fine powder of CNS was carbonized at a mild temperature of 800 °C under the nitrogen atmosphere for 3 h in a tubular furnace. After the completion carbonization process, the furnace was allowed to cool down to room temperature, and the resulting fine black powder was collected for further analysis. The detailed synthesis process of H-PCM was described in Scheme 1.



Scheme 1. Synthesis of biomass-derived heteroatom-doped porous carbon material by simple pyrolysis and their eco-friendly energy applications.

4. Conclusions

Here, an easy and cost-effective metal-free electrocatalyst was established using waste biomass of CNS via a one-pot pyrolysis route and utilized for HER in an acidic medium. The heteroatoms such as oxygen, nitrogen, and sulfur species are uniformly distributed as well as chemically bonded in the biomass-derived porous carbon matrix. The obtained H-PCM exhibits a moderate degree of crystallinity with abundant functionalities. Notably, the synthesized H-PCM possessed a high BET surface area of 565 m² g⁻¹. The exhibited porous structures with interconnected channels not only support the transportation/penetration of electrolytes but also the bubbles produced are rapidly released during the HER process. Furthermore, the nitrogen and sulfur doping in the porous carbon matrix played an essential role in the improved electrochemical conductivity during HER. Such outstanding specific characterization of H-PCM bestows the excellent electro-catalytic activity for HER in the acidic electrolyte (0.5 M H₂SO₄ aqueous solution), and the H-PCM displayed a lower Tafel slope (75 mV dec⁻¹) and excellent long-lasting durability. This work demonstrates a facile strategy to design the waste biomass-based H-PCM electrocatalysts by simple pyrolysis for HER applications and will also be extended in essential energy-related applications.

Supplementary Materials: The following are available online at <https://www.mdpi.com/article/10.3390/catal13030542/s1>. Materials, instrumentation methods, and fabrication of working electrode and electrochemical measurements of the synthesized H-PCM, Figure S1: XRD pattern of synthesized H-PCM; Figure S2: ATR-FTIR spectrum of synthesized H-PCM; Figure S3: XPS survey scan spectrum (inset of Pie chart: presented elements with atomic %) of synthesized H-PCM; Figure S4: Nitrogen sorption isotherms of synthesized H-PCM under standard temperature and pressure; Figure S5: HER polarization (LSV) curves for bare platinum plate, H-PCM/CC, and bare carbon cloth electrodes in 0.5 M H₂SO₄ aqueous solution at a scan rate of 10 mV s⁻¹; Figure S6: EIS Nyquist plots of synthesized H-PCM electrode obtained before and after prolonged stability.

Author Contributions: Conceptualization, methodology, formal analysis, investigation, data curation, and writing—original draft, R.A.; writing—review and editing and visualization, S.P.; formal analysis and investigation T.N.J.I.E.; investigation and visualization, A.K.S.; formal analysis and investigation, N.K.; visualization, S.S.; investigation, S.T.C.; project administration and supervision, Y.R.L. All authors equally contributed to this work. All authors have read and agreed to the published version of the manuscript.

Funding: This research received no external funding.

Data Availability Statement: Not applicable.

Conflicts of Interest: The authors declare no conflict of interest.

References

1. Li, Y.; Wang, H.; Priest, C.; Li, S.; Xu, P.; Wu, G. Advanced Electrocatalysis for Energy and Environmental Sustainability via Water and Nitrogen Reactions. *Adv. Mater.* **2021**, *33*, 2000381. [[CrossRef](#)] [[PubMed](#)]
2. Kaeffer, N.; Leitner, W. Electrocatalysis with Molecular Transition-Metal Complexes for Reductive Organic Synthesis. *JACS Au* **2022**, *2*, 1266–1289. [[CrossRef](#)] [[PubMed](#)]
3. Linnemann, J.; Kanokkanchana, K.; Tschulik, K. Design Strategies for Electrocatalysts from an Electrochemist's Perspective. *ACS Catal.* **2021**, *11*, 5318–5346. [[CrossRef](#)]
4. Chen, G.; Wei, C.; Zhu, Y.; Huang, H. Emerging chemical driving force in electro-catalytic water splitting. *EcoMat* **2023**, *5*, e12294. [[CrossRef](#)]
5. Edison, T.N.J.I.; Atchudan, R.; Karthik, N.; Chandrasekaran, S.; Perumal, S.; Raja, P.B.; Perumal, V.; Lee, Y.R. Deep eutectic solvent assisted electrosynthesis of ruthenium nanoparticles on stainless steel mesh for electro-catalytic hydrogen evolution reaction. *Fuel* **2021**, *297*, 120786. [[CrossRef](#)]
6. Atchudan, R.; Perumal, S.; Jebakumar Immanuel Edison, T.N.; Aldawood, S.; Vinodh, R.; Sundramoorthy, A.K.; Ghodake, G.; Lee, Y.R. Facile synthesis of novel molybdenum disulfide decorated banana peel porous carbon electrode for hydrogen evolution reaction. *Chemosphere* **2022**, *307*, 135712. [[CrossRef](#)]
7. Jebakumar Immanuel Edison, T.N.; Atchudan, R.; Karthik, N.; Lee, Y.R. Green synthesized N-doped graphitic carbon sheets coated carbon cloth as efficient metal free electrocatalyst for hydrogen evolution reaction. *Int. J. Hydrogen Energy* **2017**, *42*, 14390–14399. [[CrossRef](#)]
8. Li, Z.; Ge, R.; Su, J.; Chen, L. Recent Progress in Low Pt Content Electrocatalysts for Hydrogen Evolution Reaction. *Adv. Mater. Interfaces* **2020**, *7*, 2000396. [[CrossRef](#)]
9. Li, D.Y.; Liao, L.L.; Zhou, H.Q.; Zhao, Y.; Cai, F.M.; Zeng, J.S.; Liu, F.; Wu, H.; Tang, D.S.; Yu, F. Highly active non-noble electrocatalyst from Co₂P/Ni₂P nanohybrids for pH-universal hydrogen evolution reaction. *Mater. Today Phys.* **2021**, *16*, 100314. [[CrossRef](#)]
10. Wei, Q.; Tong, X.; Zhang, G.; Qiao, J.; Gong, Q.; Sun, S. Nitrogen-Doped Carbon Nanotube and Graphene Materials for Oxygen Reduction Reactions. *Catalysts* **2015**, *5*, 1574–1602. [[CrossRef](#)]
11. Long, G.-F.; Wan, K.; Liu, M.-Y.; Liang, Z.-X.; Piao, J.-H.; Tsiakaras, P. Active sites and mechanism on nitrogen-doped carbon catalyst for hydrogen evolution reaction. *J. Catal.* **2017**, *348*, 151–159. [[CrossRef](#)]
12. Qu, K.; Zheng, Y.; Zhang, X.; Davey, K.; Dai, S.; Qiao, S.Z. Promotion of Electro-catalytic Hydrogen Evolution Reaction on Nitrogen-Doped Carbon Nanosheets with Secondary Heteroatoms. *ACS Nano* **2017**, *11*, 7293–7300. [[CrossRef](#)] [[PubMed](#)]
13. Onyancha, R.B.; Ukhurebor, K.E.; Aigbe, U.O.; Osibote, O.A.; Kusuma, H.S.; Darmokoesoemo, H. A Methodical Review on Carbon-Based Nanomaterials in Energy-Related Applications. *Adsorpt. Sci. Technol.* **2022**, *2022*, 4438286. [[CrossRef](#)]
14. Falcao, E.H.; Wudl, F. Carbon allotropes: Beyond graphite and diamond. *J. Chem. Technol. Biotechnol.* **2007**, *82*, 524–531. [[CrossRef](#)]
15. Okwundu, O.S.; Aniekwe, E.U.; Nwanno, C.E. Unlimited potentials of carbon: Different structures and uses (a Review). *Metall. Mater. Eng.* **2018**, *24*, 145–171. [[CrossRef](#)]
16. Arul, V.; Edison, T.N.J.I.; Lee, Y.R.; Sethuraman, M.G. Biological and catalytic applications of green synthesized fluorescent N-doped carbon dots using *Hylocereus undatus*. *J. Photochem. Photobiol. B Biol.* **2017**, *168*, 142–148. [[CrossRef](#)] [[PubMed](#)]

17. Chattopadhyay, J.; Pathak, T.S.; Pak, D. Heteroatom-Doped Metal-Free Carbon Nanomaterials as Potential Electrocatalysts. *Molecules* **2022**, *27*, 670. [[CrossRef](#)]
18. Nakate, Y.T.; Sangale, S.S.; Shaikh, S.F.; Shinde, N.M.; Shirale, D.J.; Mane, R.S. Human urine-derived naturally heteroatom doped highly porous carbonaceous material for gas sensing and supercapacitor applications. *Ceram. Int.* **2022**, *48*, 28942–28950. [[CrossRef](#)]
19. Kurian, M.; Paul, A. Recent trends in the use of green sources for carbon dot synthesis—A short review. *Carbon Trends* **2021**, *3*, 100032. [[CrossRef](#)]
20. Fan, H.; Zhang, M.; Bhandari, B.; Yang, C.-H. Food waste as a carbon source in carbon quantum dots technology and their applications in food safety detection. *Trends Food Sci. Technol.* **2020**, *95*, 86–96. [[CrossRef](#)]
21. Sun, Q.; Wu, Z.; Cao, B.; Chen, X.; Zhang, C.; Shaymurat, T.; Duan, H.; Zhang, J.; Zhang, M. Gas sensing performance of biomass carbon materials promoted by nitrogen doping and p-n junction. *Appl. Surf. Sci.* **2022**, *592*, 153254. [[CrossRef](#)]
22. Sekhon, S.S.; Park, J.-S. Biomass-derived N-doped porous carbon nanosheets for energy technologies. *Chem. Eng. J.* **2021**, *425*, 129017. [[CrossRef](#)]
23. Matsagar, B.M.; Yang, R.-X.; Dutta, S.; Ok, Y.S.; Wu, K.C.W. Recent progress in the development of biomass-derived nitrogen-doped porous carbon. *J. Mater. Chem. A* **2021**, *9*, 3703–3728. [[CrossRef](#)]
24. Liu, X.; Zhou, W.; Yang, L.; Li, L.; Zhang, Z.; Ke, Y.; Chen, S. Nitrogen and sulfur co-doped porous carbon derived from human hair as highly efficient metal-free electrocatalysts for hydrogen evolution reactions. *J. Mater. Chem. A* **2015**, *3*, 8840–8846. [[CrossRef](#)]
25. Ito, Y.; Cong, W.; Fujita, T.; Tang, Z.; Chen, M. High Catalytic Activity of Nitrogen and Sulfur Co-Doped Nanoporous Graphene in the Hydrogen Evolution Reaction. *Angew. Chem. Int. Ed.* **2015**, *54*, 2131–2136. [[CrossRef](#)]
26. Iravani, S.; Varma, R.S. Green synthesis, biomedical and biotechnological applications of carbon and graphene quantum dots. A review. *Environ. Chem. Lett.* **2020**, *18*, 703–727. [[CrossRef](#)]
27. Murugesan, C.; Senthilkumar, B.; Barpanda, P. Biowaste-Derived Highly Porous N-Doped Carbon as a Low-Cost Bifunctional Electrocatalyst for Hybrid Sodium–Air Batteries. *ACS Sustain. Chem. Eng.* **2022**, *10*, 9077–9086. [[CrossRef](#)]
28. Li, Z.; Bai, Z.; Mi, H.; Ji, C.; Gao, S.; Pang, H. Biowaste-Derived Porous Carbon with Tuned Microstructure for High-Energy Quasi-Solid-State Supercapacitors. *ACS Sustain. Chem. Eng.* **2019**, *7*, 13127–13135. [[CrossRef](#)]
29. Li, Y.; Xu, R.; Wang, B.; Wei, J.; Wang, L.; Shen, M.; Yang, J. Enhanced N-doped Porous Carbon Derived from KOH-Activated Waste Wool: A Promising Material for Selective Adsorption of CO₂/CH₄ and CH₄/N₂. *Nanomaterials* **2019**, *9*, 266. [[CrossRef](#)]
30. Du, J.; Zhang, Y.; Lv, H.; Chen, A. Silicate-assisted activation of biomass towards N-doped porous carbon sheets for supercapacitors. *J. Alloys Compd.* **2021**, *853*, 157091. [[CrossRef](#)]
31. Chen, M.; Jiang, S.; Huang, C.; Wang, X.; Cai, S.; Xiang, K.; Zhang, Y.; Xue, J. Honeycomb-like Nitrogen and Sulfur Dual-Doped Hierarchical Porous Biomass-Derived Carbon for Lithium–Sulfur Batteries. *ChemSusChem* **2017**, *10*, 1803–1812. [[CrossRef](#)] [[PubMed](#)]
32. Guan, Z.; Guan, Z.; Li, Z.; Liu, J.; Yu, K. Characterization and Preparation of Nano-porous Carbon Derived from Hemp Stems as Anode for Lithium-Ion Batteries. *Nanoscale Res. Lett.* **2019**, *14*, 338. [[CrossRef](#)] [[PubMed](#)]
33. Shang, H.; Lu, Y.; Zhao, F.; Chao, C.; Zhang, B.; Zhang, H. Preparing high surface area porous carbon from biomass by carbonization in a molten salt medium. *RSC Adv.* **2015**, *5*, 75728–75734. [[CrossRef](#)]
34. Atchudan, R.; Perumal, S.; Edison, T.N.J.I.; Sundramoorthy, A.K.; Sangaraju, S.; Babu, R.S.; Lee, Y.R. Sustainable Synthesis of Bright Fluorescent Nitrogen-Doped Carbon Dots from Terminalia chebula for In Vitro Imaging. *Molecules* **2022**, *27*, 8085. [[CrossRef](#)]
35. Lei, W.; Liu, H.; Xiao, J.; Wang, Y.; Lin, L. Moss-Derived Mesoporous Carbon as Bi-Functional Electrode Materials for Lithium–Sulfur Batteries and Supercapacitors. *Nanomaterials* **2019**, *9*, 84. [[CrossRef](#)]
36. Yang, S.; Zhang, K. Converting Corn cob to Activated Porous Carbon for Supercapacitor Application. *Nanomaterials* **2018**, *8*, 181. [[CrossRef](#)] [[PubMed](#)]
37. Wei, C.; Yu, J.; Yang, X.; Zhang, G. Activated Carbon Fibers with Hierarchical Nanostructure Derived from Waste Cotton Gloves as High-Performance Electrodes for Supercapacitors. *Nanoscale Res. Lett.* **2017**, *12*, 379. [[CrossRef](#)]
38. Perumal, S.; Atchudan, R.; Ramalingam, S.; Aldawood, S.; Devarajan, N.; Lee, W.; Lee, Y.R. Silver nanoparticles loaded graphene-poly-vinylpyrrolidone composites as an effective recyclable antimicrobial agent. *Environ. Res.* **2023**, *216*, 114706. [[CrossRef](#)]
39. Perumal, S.; Atchudan, R.; Lee, Y.R. Synthesis of Water-Dispersed Sulfobetaine Methacrylate–Iron Oxide Nanoparticle-Coated Graphene Composite by Free Radical Polymerization. *Polymers* **2022**, *14*, 3885.
40. Kaniyoor, A.; Ramaprabhu, S. A Raman spectroscopic investigation of graphite oxide derived graphene. *AIP Adv.* **2012**, *2*, 032183. [[CrossRef](#)]
41. Liu, H.; Zhang, Y.; Huang, C. Development of nitrogen and sulfur-doped carbon dots for cellular imaging. *J. Pharm. Anal.* **2019**, *9*, 127–132. [[CrossRef](#)]
42. Zhou, H.; Ren, Y.; Li, Z.; He, W.; Li, Z. Selective Detection of Fe³⁺ by Nitrogen–Sulfur-Doped Carbon Dots Using Thiourea and Citric Acid. *Coatings* **2022**, *12*, 1042. [[CrossRef](#)]
43. Kundoo, S.; Saha, P.; Chattopadhyay, K.K. Electron field emission from nitrogen and sulfur-doped diamond-like carbon films deposited by simple electrochemical route. *Mater. Lett.* **2004**, *58*, 3920–3924. [[CrossRef](#)]

44. Zhu, S.; Wang, K.; Hu, J.; Liu, R.; Zhu, H. Nitrogen and sulphur co-doped carbon quantum dots and their optical power limiting properties. *Mater. Adv.* **2020**, *1*, 3176–3181. [[CrossRef](#)]
45. Atchudan, R.; Perumal, S.; Edison, T.N.J.I.; Albasher, G.; Sundramoorthy, A.K.; Vinodh, R.; Lee, Y.R. Lotus-biowaste derived sulfur/nitrogen-codoped porous carbon as an eco-friendly electrocatalyst for clean energy harvesting. *Environ. Res.* **2022**, *214*, 113910. [[CrossRef](#)]
46. Ouyang, Z.; Lei, Y.; Chen, Y.; Zhang, Z.; Jiang, Z.; Hu, J.; Lin, Y. Preparation and Specific Capacitance Properties of Sulfur, Nitrogen Co-Doped Graphene Quantum Dots. *Nanoscale Res. Lett.* **2019**, *14*, 219. [[CrossRef](#)]
47. Sun, C.; Zhang, Y.; Wang, P.; Yang, Y.; Wang, Y.; Xu, J.; Wang, Y.; Yu, W.W. Synthesis of Nitrogen and Sulfur Co-doped Carbon Dots from Garlic for Selective Detection of Fe³⁺. *Nanoscale Res. Lett.* **2016**, *11*, 110. [[CrossRef](#)]
48. Xue, M.; Zhang, L.; Zou, M.; Lan, C.; Zhan, Z.; Zhao, S. Nitrogen and sulfur co-doped carbon dots: A facile and green fluorescence probe for free chlorine. *Sens. Actuators B Chem.* **2015**, *219*, 50–56. [[CrossRef](#)]
49. Guo, Z.; Feng, X.; Li, X.; Zhang, X.; Peng, X.; Song, H.; Fu, J.; Ding, K.; Huang, X.; Gao, B. Nitrogen Doped Carbon Nanosheets Encapsulated in situ Generated Sulfur Enable High Capacity and Superior Rate Cathode for Li-S Batteries. *Front. Chem.* **2018**, *6*, 429. [[CrossRef](#)]
50. Ilnicka, A.; Skorupska, M.; Tyc, M.; Kowalska, K.; Kamedulski, P.; Zielinski, W.; Lukaszewicz, J.P. Green algae and gelatine derived nitrogen rich carbon as an outstanding competitor to Pt loaded carbon catalysts. *Sci. Rep.* **2021**, *11*, 7084. [[CrossRef](#)]
51. Fechler, N.; Fellingner, T.-P.; Antonietti, M. One-pot synthesis of nitrogen–sulfur-co-doped carbons with tunable composition using a simple isothiocyanate ionic liquid. *J. Mater. Chem. A* **2013**, *1*, 14097–14102. [[CrossRef](#)]
52. Atchudan, R.; Chandra Kishore, S.; Gangadaran, P.; Jebakumar Immanuel Edison, T.N.; Perumal, S.; Rajendran, R.L.; Alagan, M.; Al-Rashed, S.; Ahn, B.-C.; Lee, Y.R. Tunable fluorescent carbon dots from biowaste as fluorescence ink and imaging human normal and cancer cells. *Environ. Res.* **2022**, *204*, 112365. [[CrossRef](#)] [[PubMed](#)]
53. Karikalan, N.; Velmurugan, M.; Chen, S.-M.; Karuppiyah, C. Modern Approach to the Synthesis of Ni(OH)₂ Decorated Sulfur Doped Carbon Nanoparticles for the Nonenzymatic Glucose Sensor. *ACS Appl. Mater. Interfaces* **2016**, *8*, 22545–22553. [[CrossRef](#)] [[PubMed](#)]
54. Xu, J.; Su, D.; Zhang, W.; Bao, W.; Wang, G. A nitrogen–sulfur co-doped porous graphene matrix as a sulfur immobilizer for high performance lithium–sulfur batteries. *J. Mater. Chem. A* **2016**, *4*, 17381–17393. [[CrossRef](#)]
55. Zhang, J.; Wang, J.; Wu, Z.; Wang, S.; Wu, Y.; Liu, X. Heteroatom (Nitrogen/Sulfur)-Doped Graphene as an Efficient Electrocatalyst for Oxygen Reduction and Evolution Reactions. *Catalysts* **2018**, *8*, 475. [[CrossRef](#)]
56. Chen, H.; Yu, F.; Wang, G.; Chen, L.; Dai, B.; Peng, S. Nitrogen and Sulfur Self-Doped Activated Carbon Directly Derived from Elm Flower for High-Performance Supercapacitors. *ACS Omega* **2018**, *3*, 4724–4732. [[CrossRef](#)]
57. Ji, H.; Wang, T.; Liu, Y.; Lu, C.; Yang, G.; Ding, W.; Hou, W. A novel approach for sulfur-doped hierarchically porous carbon with excellent capacitance for electrochemical energy storage. *Chem. Commun.* **2016**, *52*, 12725–12728. [[CrossRef](#)] [[PubMed](#)]
58. Song, W.; Kan, J.; Wang, H.; Zhao, X.; Zheng, Y.; Zhang, H.; Tao, L.; Huang, M.; Liu, W.; Shi, J. Nitrogen and Sulfur Co-doped Mesoporous Carbon for Sodium Ion Batteries. *ACS Appl. Nano Mater.* **2019**, *2*, 5643–5654. [[CrossRef](#)]
59. Ding, J.; He, W.; Yu, C.; Liu, Z.; Deng, C.; Zhu, H. Waste biomass derived carbon supported Mo₂C/C composite materials for heavy metal adsorption and hydrogen evolution reaction. *Mater. Today Commun.* **2022**, *31*, 103646. [[CrossRef](#)]
60. Lim, B.A.-L.; Lim, S.; Pang, Y.L.; Shuit, S.H.; Wong, K.H.; Ooi, J.B. Investigation on the Potential of Various Biomass Waste for the Synthesis of Carbon Material for Energy Storage Application. *Sustainability* **2022**, *14*, 2919. [[CrossRef](#)]
61. Zhang, H.; Zhu, Y.; Liu, Q.; Li, X. Preparation of porous carbon materials from biomass pyrolysis vapors for hydrogen storage. *Appl. Energy* **2022**, *306*, 118131. [[CrossRef](#)]
62. Min, S.; Duan, Y.; Li, Y.; Wang, F. Biomass-derived self-supported porous carbon membrane embedded with Co nanoparticles as an advanced electrocatalyst for efficient and robust hydrogen evolution reaction. *Renew. Energy* **2020**, *155*, 447–455. [[CrossRef](#)]
63. Chen, X.; Sun, J.; Guo, T.; Zhao, R.; Liu, L.; Liu, B.; Wang, Y.; Li, J.; Du, J. Biomass-derived carbon nanosheets coupled with MoO₂/Mo₂C electrocatalyst for hydrogen evolution reaction. *Int. J. Hydrogen Energy* **2022**, *47*, 30959–30969. [[CrossRef](#)]
64. Han, G.; Hu, M.; Liu, Y.; Gao, J.; Han, L.; Lu, S.; Cao, H.; Wu, X.; Li, B. Efficient carbon-based catalyst derived from natural cattail fiber for hydrogen evolution reaction. *J. Solid State Chem.* **2019**, *274*, 207–214. [[CrossRef](#)]
65. Cao, Y.; Meng, Y.; Huang, S.; He, S.; Li, X.; Tong, S.; Wu, M. Nitrogen-, Oxygen- and Sulfur-Doped Carbon-Encapsulated Ni₃S₂ and NiS Core–Shell Architectures: Bifunctional Electrocatalysts for Hydrogen Evolution and Oxygen Reduction Reactions. *ACS Sustain. Chem. Eng.* **2018**, *6*, 15582–15590. [[CrossRef](#)]
66. Zhang, L.; Yin, J.; Wei, K.; Li, B.; Jiao, T.; Chen, Y.; Zhou, J.; Peng, Q. Fabrication of hierarchical SrTiO₃@MoS₂ heterostructure nanofibers as efficient and low-cost electrocatalysts for hydrogen-evolution reactions. *Nanotechnology* **2020**, *31*, 205604. [[CrossRef](#)]
67. Chinnadurai, D.; Karuppiyah, P.; Chen, S.-M.; Kim, H.-j.; Prabakar, K. Metal-free multiporous carbon for electrochemical energy storage and electrocatalysis applications. *New J. Chem.* **2019**, *43*, 11653–11659. [[CrossRef](#)]
68. Tian, J.; Li, J.; Feng, A.; Han, X.; Lv, Y.; Ma, M.; Lin, C. Self-limited conversion of MoO₂ into ultramicro MoS₂ nanosheets on graphene/CNTs matrix for hydrogen evolution with excellent stability. *Sustain. Energy Fuels* **2020**, *4*, 2869–2874. [[CrossRef](#)]
69. Fakayode, O.A.; Yusuf, B.A.; Zhou, C.; Xu, Y.; Ji, Q.; Xie, J.; Ma, H. Simplistic two-step fabrication of porous carbon-based biomass-derived electrocatalyst for efficient hydrogen evolution reaction. *Energy Convers. Manag.* **2021**, *227*, 113628. [[CrossRef](#)]
70. Chen, H.; Jiang, H.; Cao, X.; Zhang, Y.; Zhang, X.; Qiao, S. Castoff derived Biomass—carbon supported MoS₂ nanosheets for hydrogen evolution reaction. *Mater. Chem. Phys.* **2020**, *252*, 123244. [[CrossRef](#)]

71. Hoang, V.C.; Gomes, V.G.; Dinh, K.N. Ni- and P-doped carbon from waste biomass: A sustainable multifunctional electrode for oxygen reduction, oxygen evolution and hydrogen evolution reactions. *Electrochim. Acta* **2019**, *314*, 49–60. [[CrossRef](#)]
72. Cao, X.; Li, Z.; Chen, H.; Zhang, C.; Zhang, Y.; Gu, C.; Xu, X.; Li, Q. Synthesis of biomass porous carbon materials from bean sprouts for hydrogen evolution reaction electrocatalysis and supercapacitor electrode. *Int. J. Hydrogen Energy* **2021**, *46*, 18887–18897. [[CrossRef](#)]

Disclaimer/Publisher’s Note: The statements, opinions and data contained in all publications are solely those of the individual author(s) and contributor(s) and not of MDPI and/or the editor(s). MDPI and/or the editor(s) disclaim responsibility for any injury to people or property resulting from any ideas, methods, instructions or products referred to in the content.